Electronic Supplementary Information (ESI)

Molecular sieving using metal–polymer coordination membranes in organic media

Rifan Hardian,[1] Peter Pogany,[2] Young Moo Lee,[3] Gyorgy Szekely[1,*]

[1]Advanced Membrane and Porous Materials Center, Physical Science and Engineering Division (PSE), King Abdullah University of Science and Technology (KAUST), Thuwal 23955-6900, Saudi Arabia

[2]Department of Inorganic & Analytical Chemistry, Budapest University of Technology and Economics, Szent Gellert ter 4, Budapest 1111, Hungary

[3]WCU Department of Energy Engineering, Hanyang University, Seoul 04763, Republic of Korea

*Corresponding author: gyorgy.szekely@kaust.edu.sa, www.szekelygroup.com

Table of Contents

1. Characterization S4
2. Pore size calculation S17
3. Membrane performance S20
4. References S21

List of Figures

Fig. S1. C 1s XPS spectra of the MPC membranes and their deconvolutions. S4
Fig. S2. N 1s XPS spectra of the MPC membranes and their deconvolutions S5
Fig. S3. Solid-state 13C and 1H NMR of M0 (black) and M3 (red) S6
Fig. S4. Liquid state 1H NMR of DMAc, PBI with DMAc, and the PBI–CuI–DMAc system S7
Fig. S5. ATR–FTIR spectra of the MPC membranes S7
Fig. S6. Schematic illustration of the proposed PBI structural evolution S8
Fig. S7. Reaction and product isolation of CuI in acetonitrile and benzimidazole S9
Fig. S8. Morphology analysis. SEM and AFM images of the MPC membranes S10
Fig. S9. TEM images of the MPC membranes and their EELS mapping S11
Fig. S10. Water contact angle of pelletized CuI S12
Fig. S11. Water contact angles of the MPC membranes S12
Fig. S12. TEM high magnification of M3. ..... S13
Fig. S13. SEM images of the MPC membranes and an illustration of the nanoparticles' evolution S14
Fig. S14. SEM images of the agglomerates formed in the membranes. S15
Fig. S15. Photos of the desert rose selenite S15
Fig. S16. EDX spectra of M0-M3 upon acid and base testing S16
Fig. S17. Schematic of the multistage crossflow nanofiltration apparatus used for membrane testing. S22
Fig. S18. SEM cross-section of M3 before (a) and after (b) continuous filtration test. S22
Fig. S19. High magnification of SEM cross-section of the MPC membranes S23

List of Tables

Table S1. Elemental analysis of the membranes. S16
Table S2. Membrane stability test S16
Table S3. Physical properties of acetone S17
Table S4. Physical properties of the solvents and their solvent solubility parameters. S19
Table S5. Rejection of the dyes and APIs for M3 in acetone at 30 bar. S20
Table S6. Flux of acetone through M0-M3 at 30 bar. S20
Table S7. Comparison of the filtration performance S21

1. Characterization

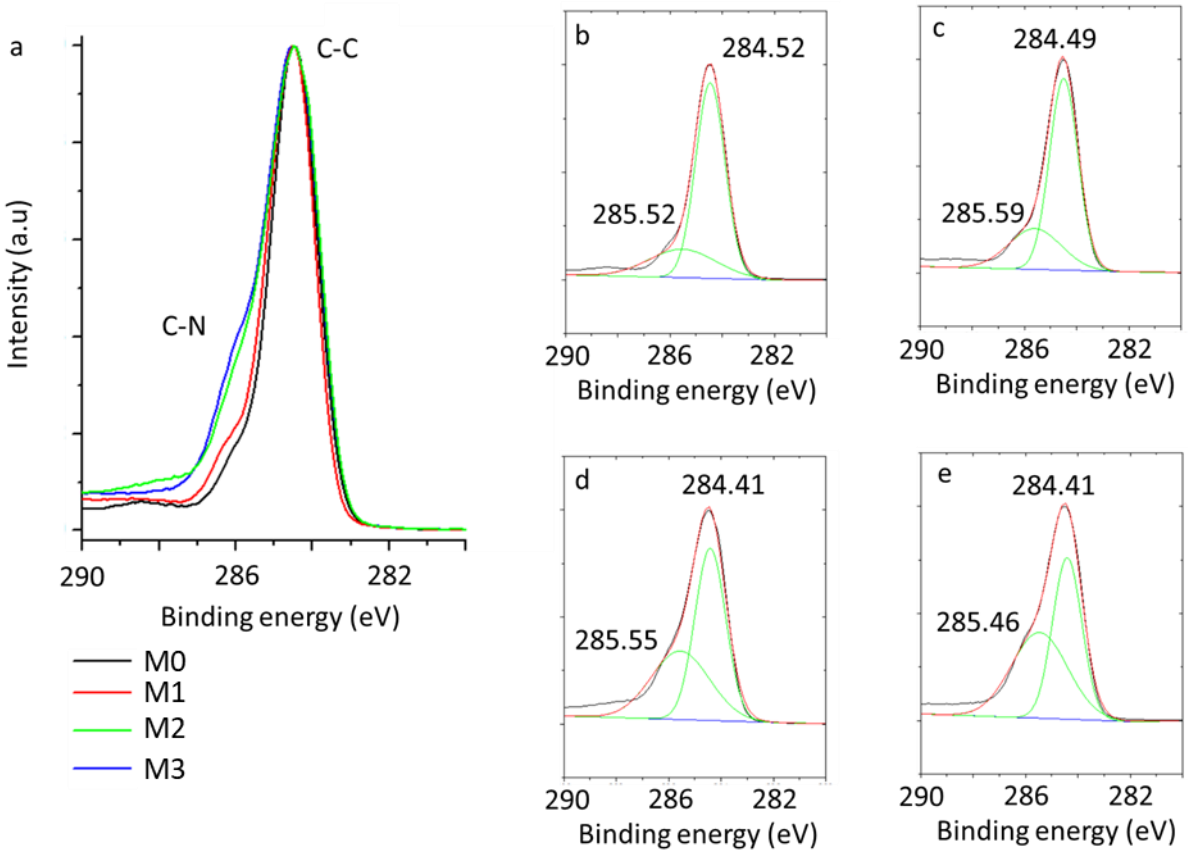

Fig. S1. C 1s XPS spectra (a) and its deconvolutions for M0 (b), M1 (c), M2 (d), and M3 (e).

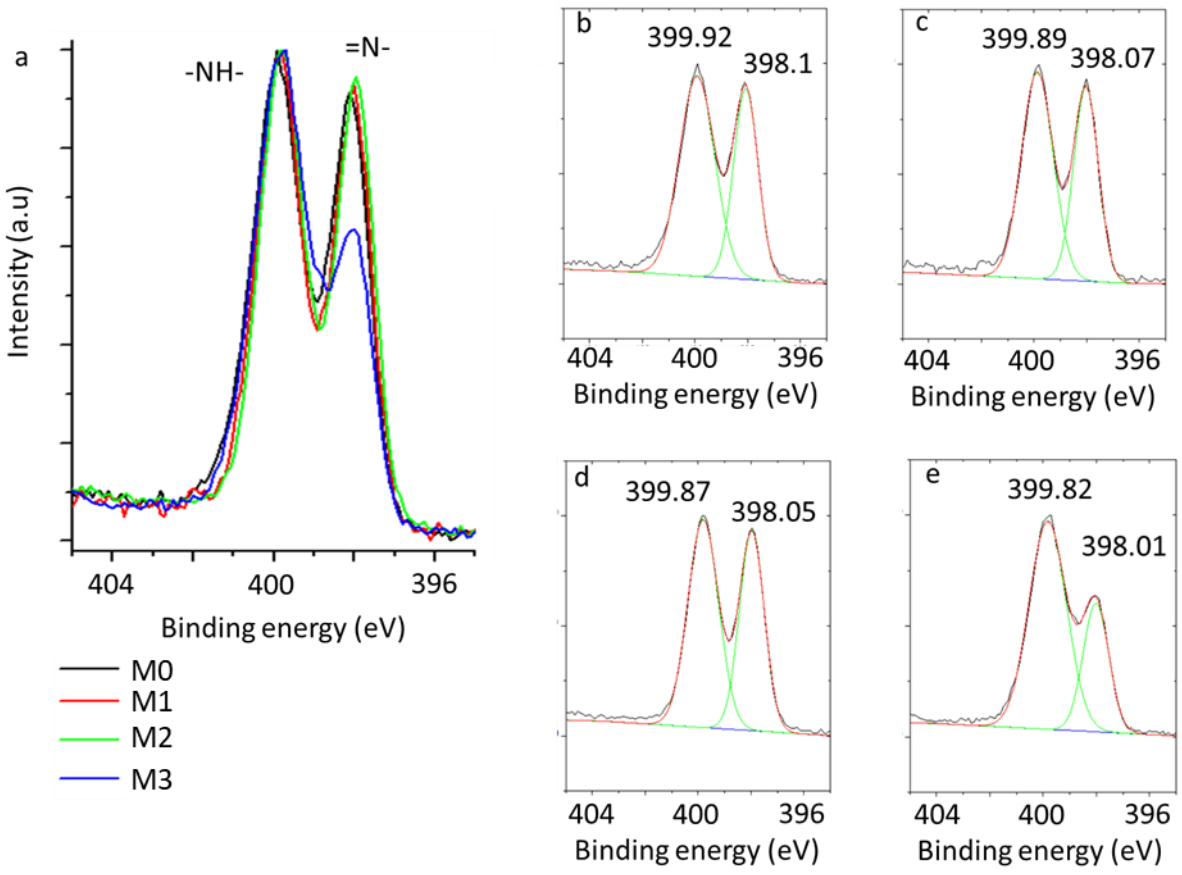

Fig. S2. N 1s XPS spectra (a) and its deconvolutions for M0 (b), M1 (c), M2 (d), and M3 (e).

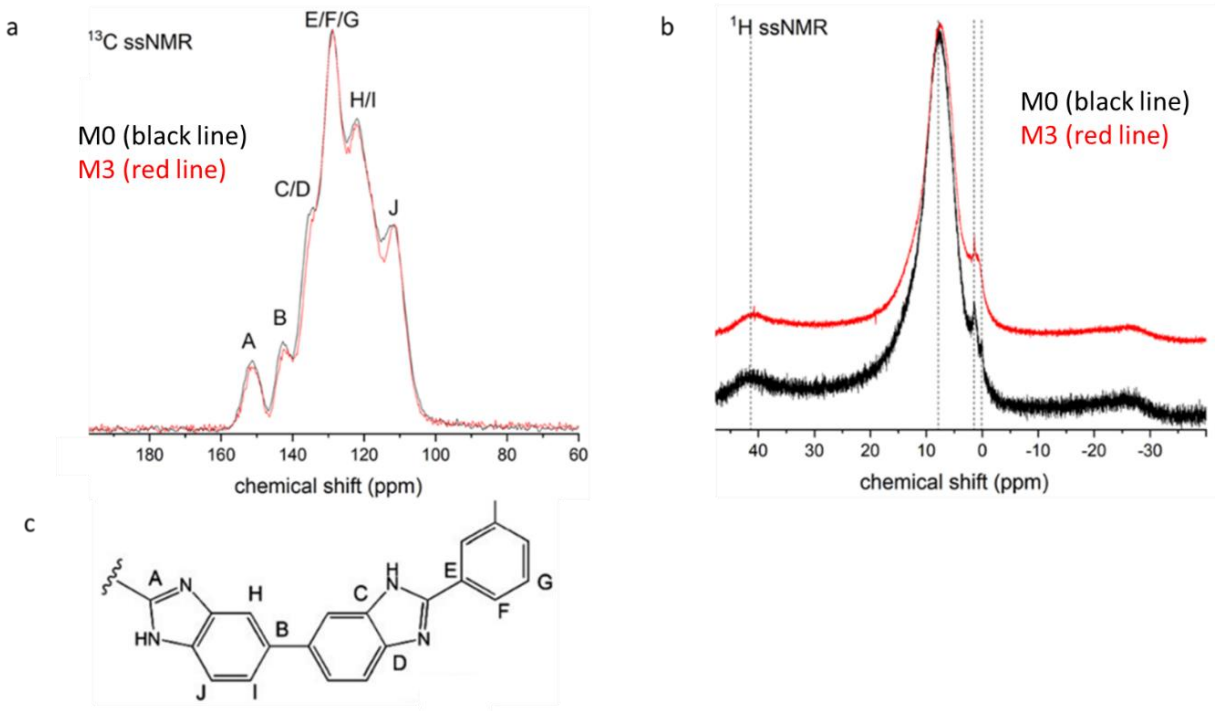

Fig. S3. Solid-state ^{13}C (a) and ^{1}H (b) NMR of M0 (black) and M3 (red). PBI structure with its corresponding carbon designation.

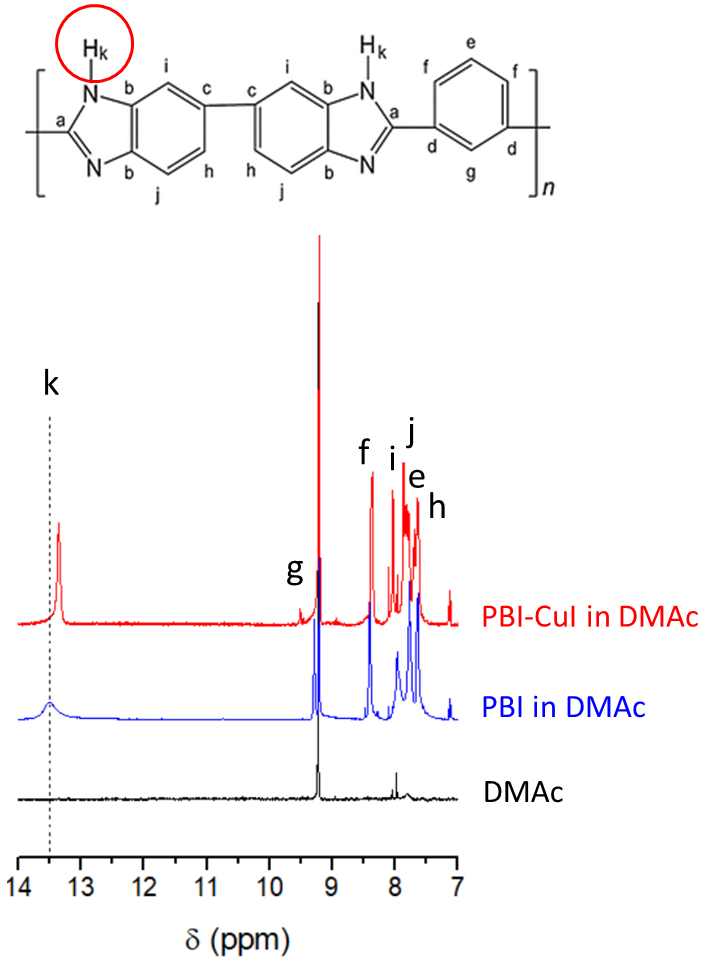

Fig. S4. Liquid state ^{1}H NMR of DMAc, PBI with DMAc, and the PBI–CuI–DMAc system.

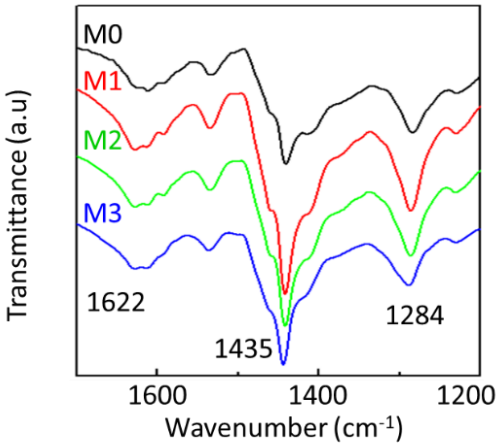

Fig. S5. ATR–FTIR spectra of M0, M1, M2, and M3. The peaks at 1622, 1435, and 1284 cm^{-1} correspond to (C=N, C=C stretching), the in-plane ring vibration of benzimidazole, and the imidazole ring breathing vibration, respectively.

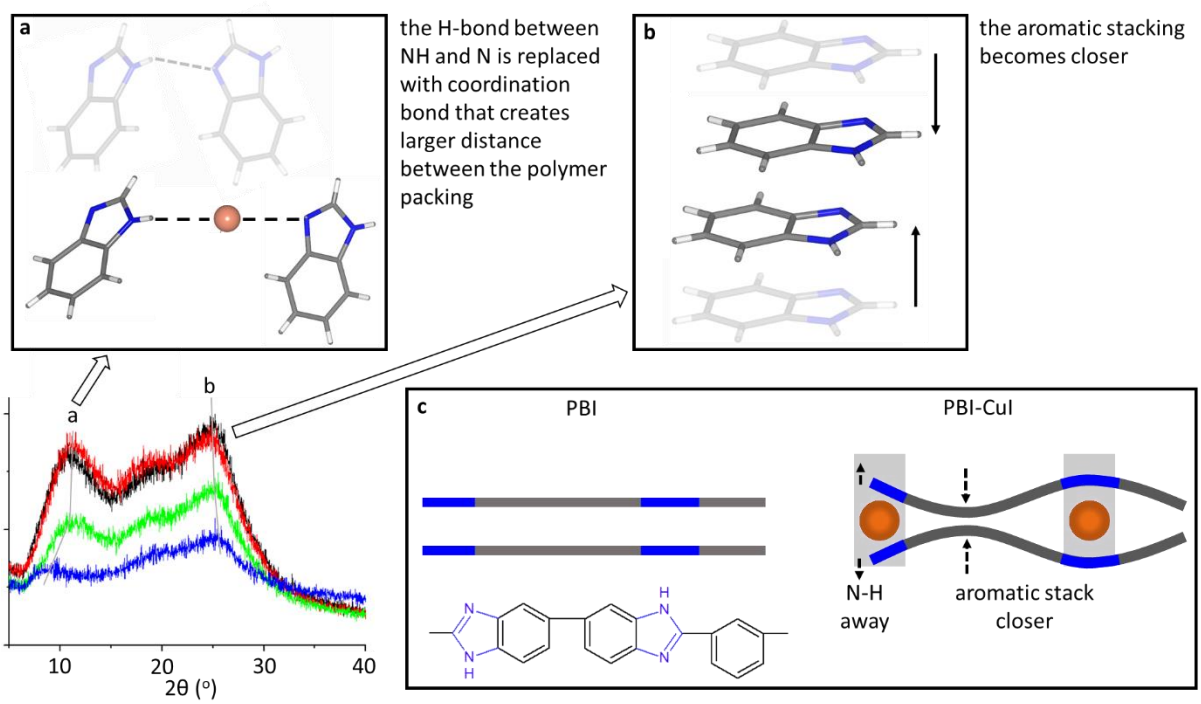

Fig. S6. Schematic illustration of the proposed PBI structural evolution. (a) The hydrogen bonding between NH and N in the imidazole became further away because of the insertion of the CuI molecule. (b) The aromatic ring stacking became closer. (c) The proposed polymer chain arrangement in the PBI before and after CuI coordination.

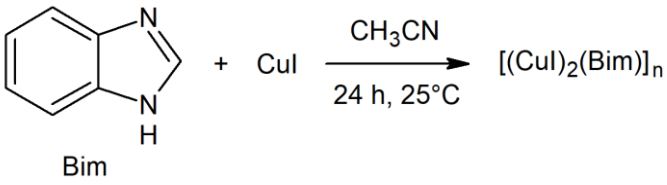

Scheme S1. Reaction between benzimidazole and CuI in acetonitrile at room temperature.

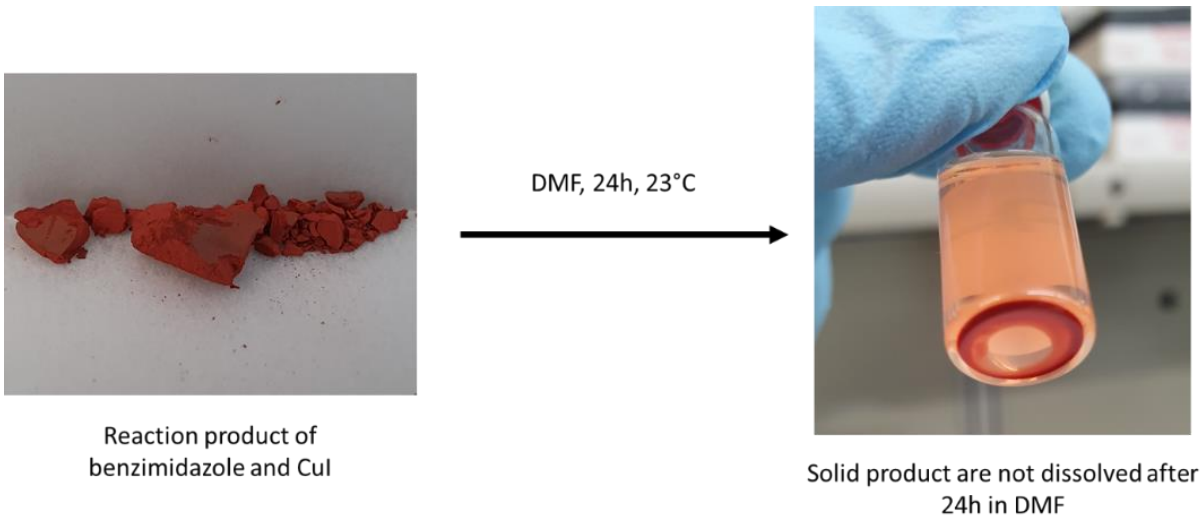

Fig. S7. Reaction and product isolation of CuI in acetonitrile and benzimidazole at room temperature.

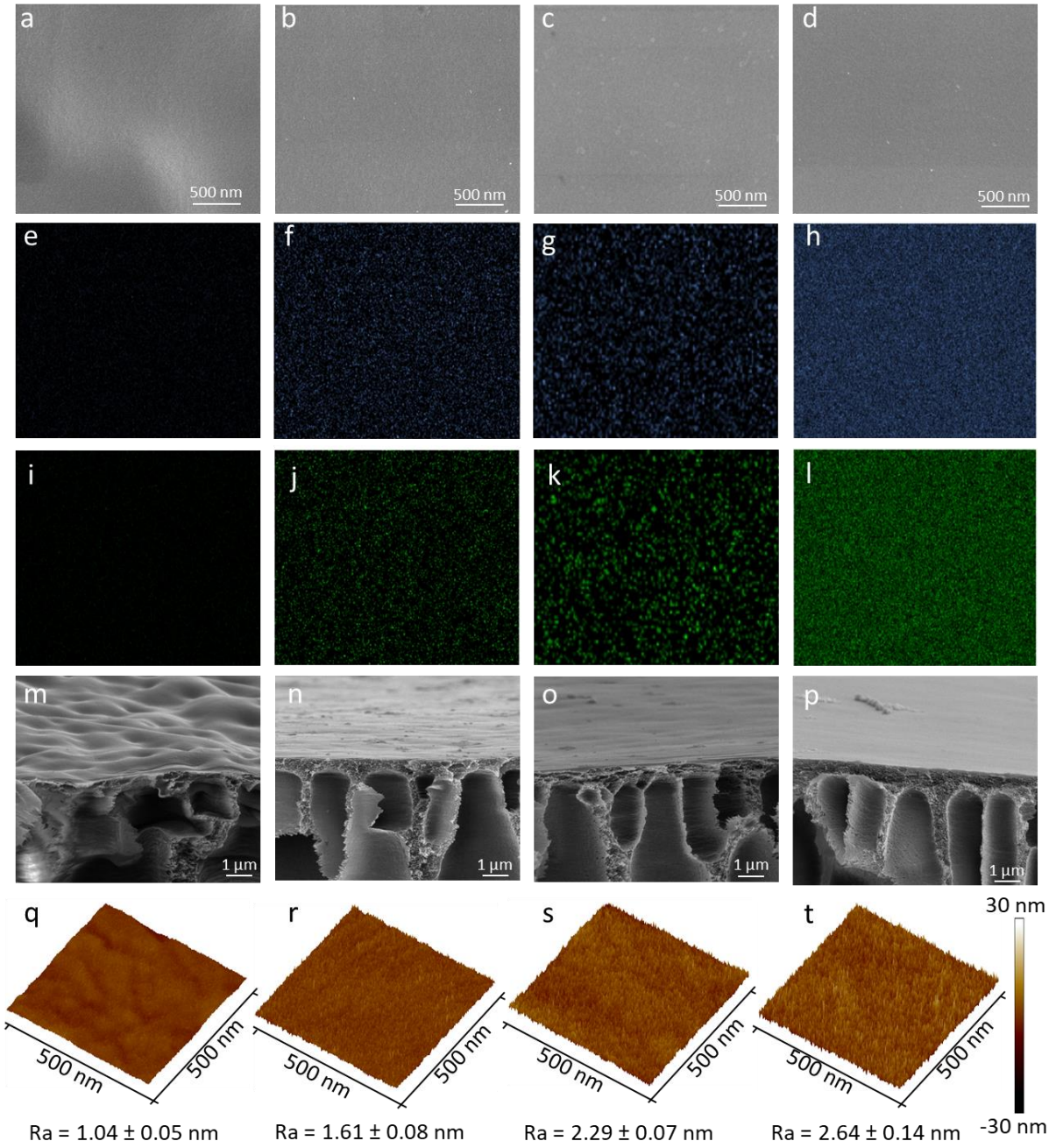

Fig. S8. Morphology analysis. SEM membrane surfaces of M0 (a), M1 (b), M2 (c), and M3 (d). EDX mapping of iodine (blue dots) and copper (green dots) on the surfaces of M0 (e,i), M1 (f,j), M2 (g,k), and M3 (h,l). SEM cross-section images of M0 (m), M1 (n), M2 (o), and M3 (p). AFM height images (scan size = 500 × 500 nm) of the M0 (q), M1 (r), M2 (s), and M3 (t) membranes.

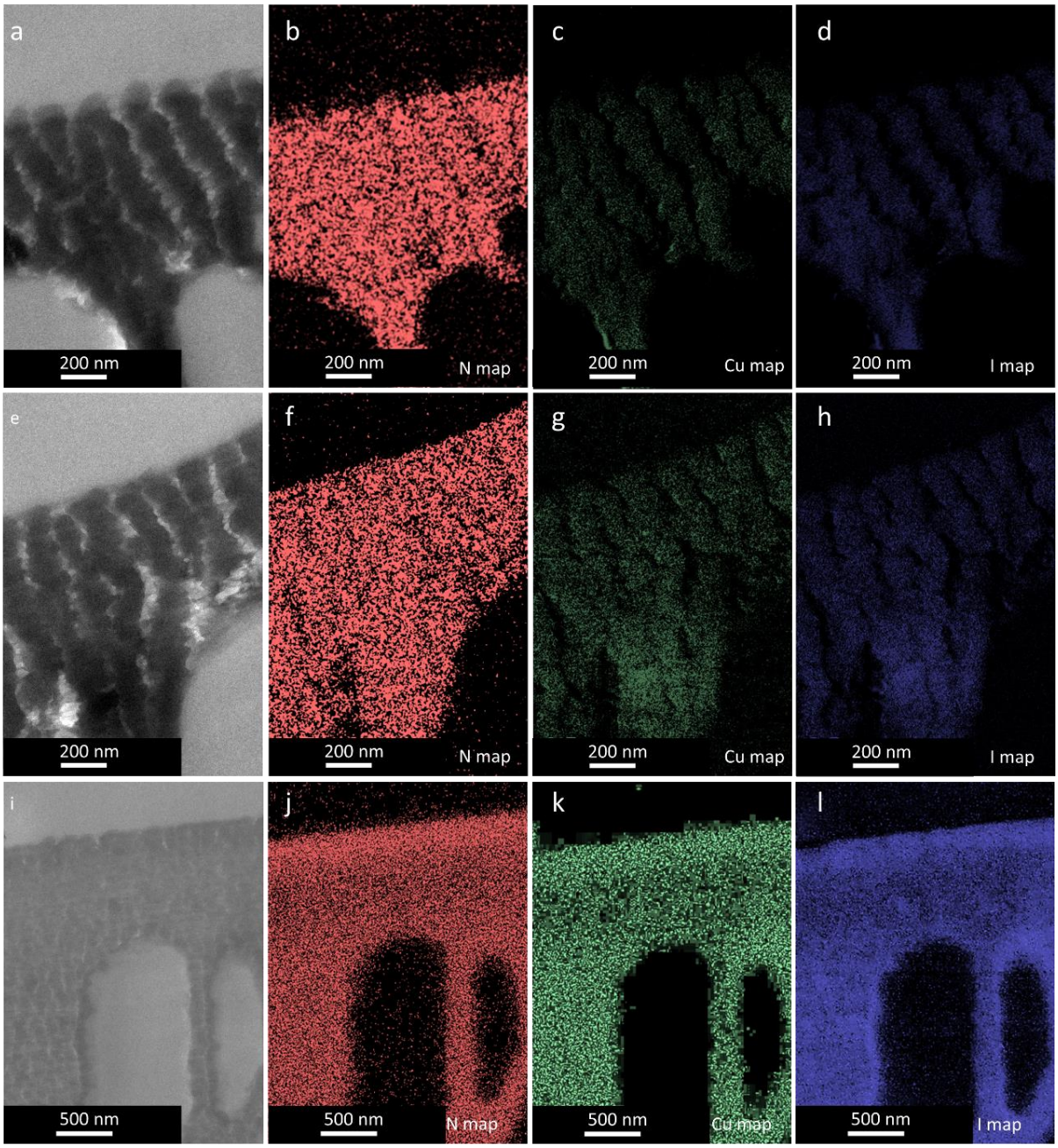

Fig. S9. TEM high-magnification images of M1 (a), M2 (e), and M3 (i). EELS mapping on M1(b-d), M2 (f-h), and M3 (j-l).

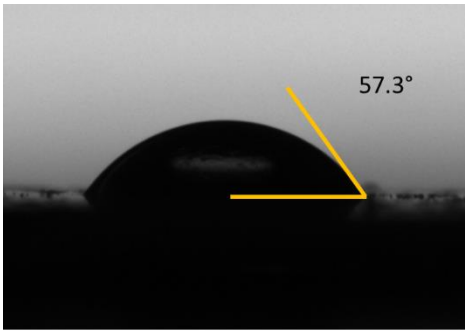

Fig. S10. Contact angle of pelletized CuI.

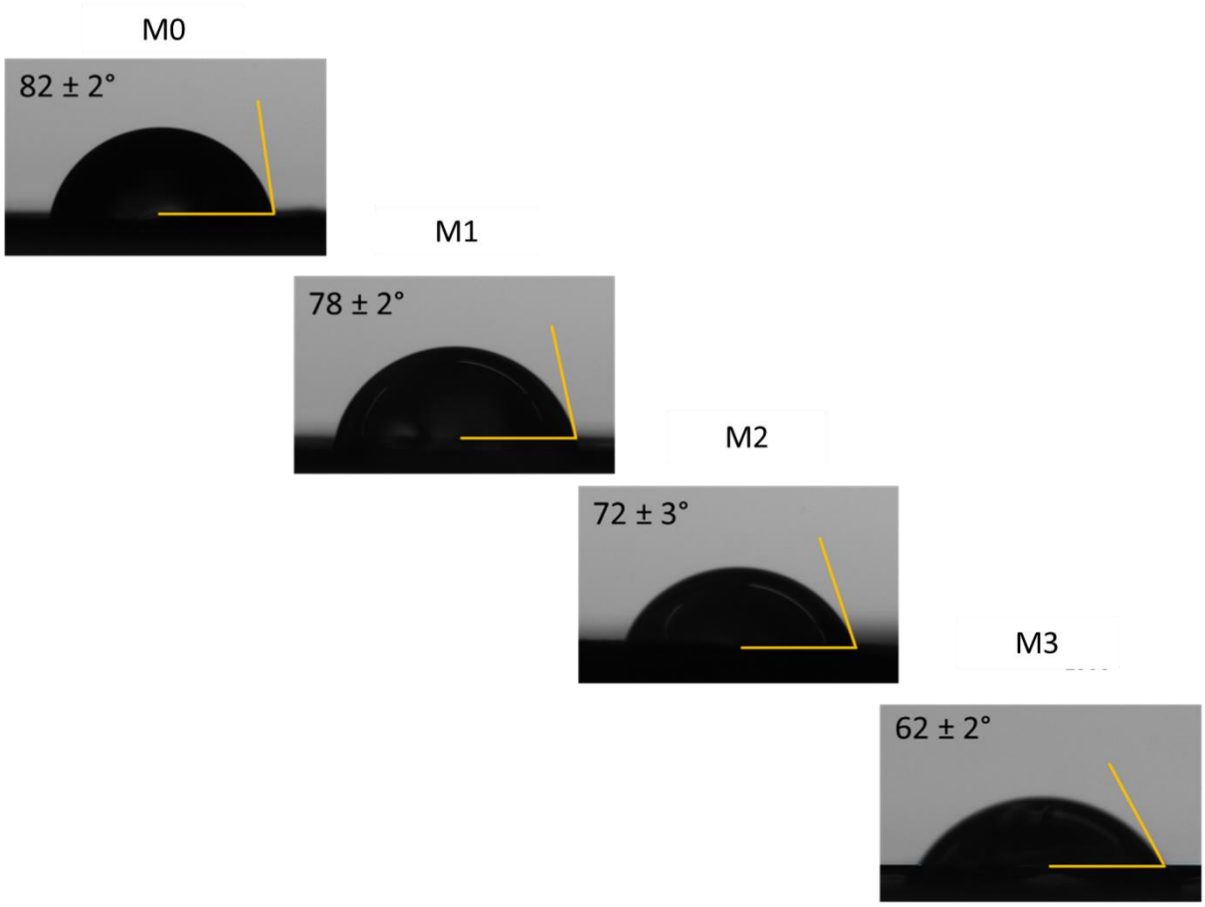

Fig. S11. Water contact angles of the M0, M1, M2, and M3 membranes.

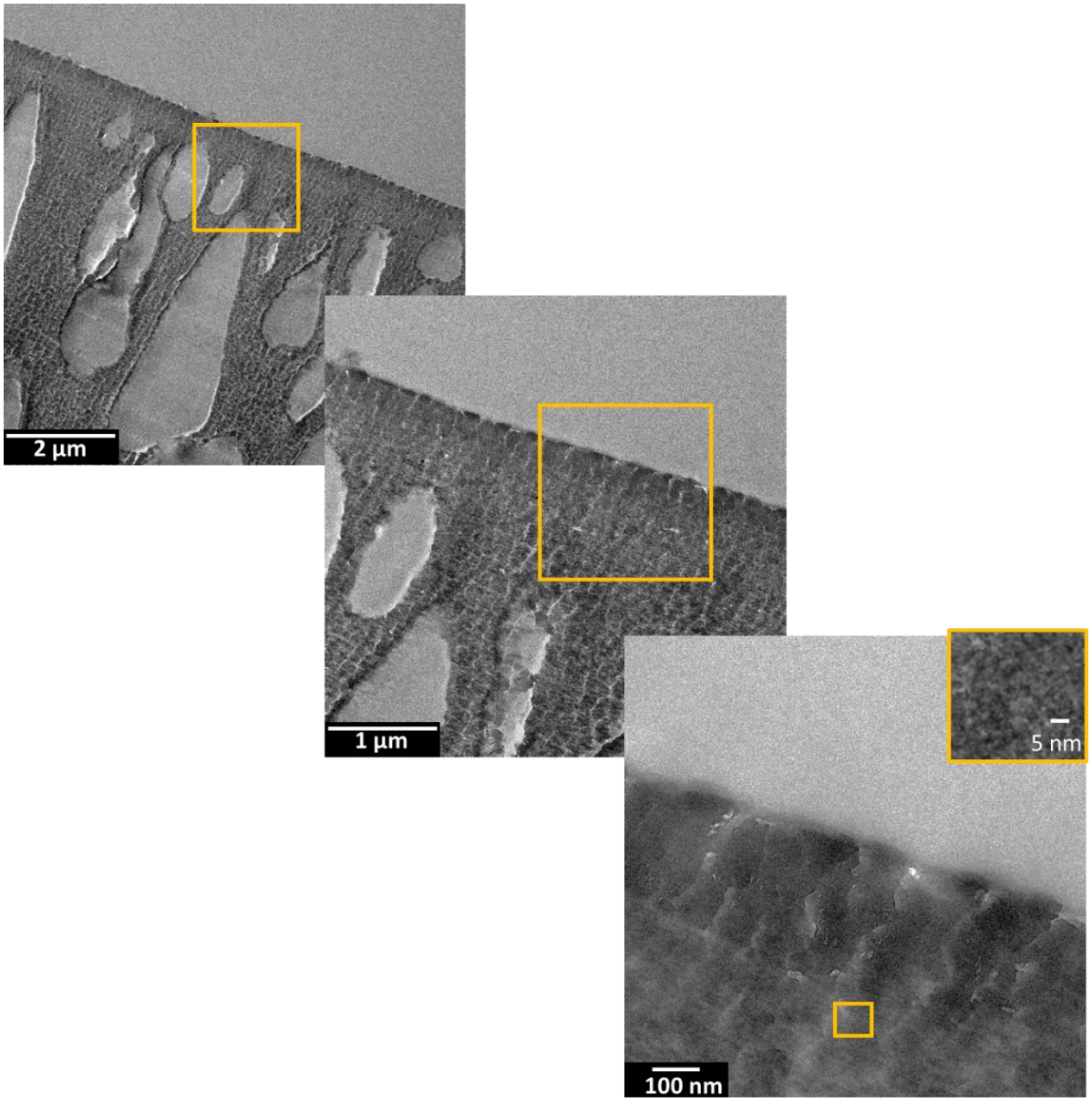

Fig. S12. TEM high magnification of M3. No particle formation was observed.

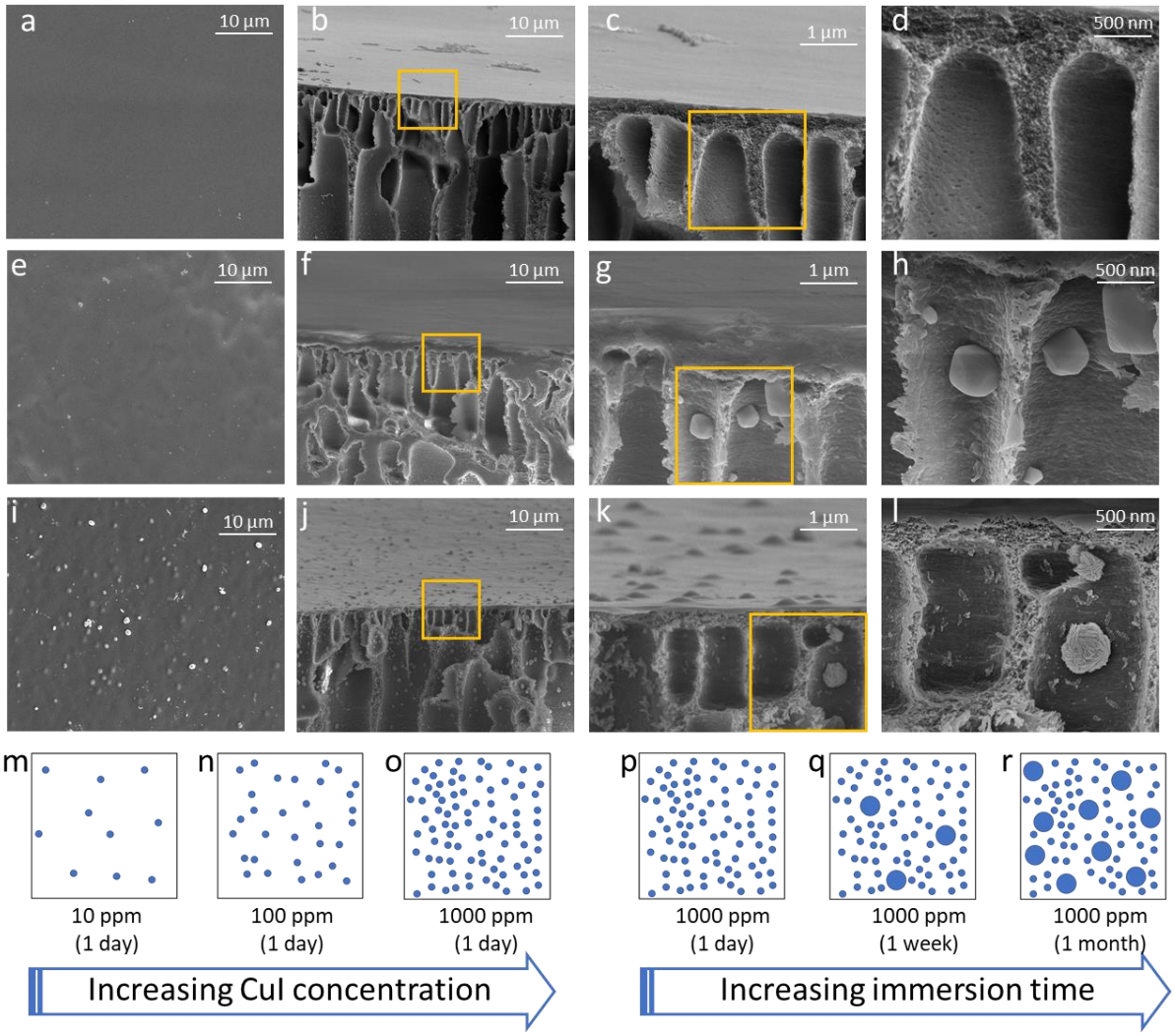

Fig. S13. SEM images (surface and cross-section) of M3 with treatment durations of 1 day (a-d), 1 week (e-h), and 1 month (i-l). Illustration of the nanoparticle evolution upon increasing the concentration (m-o) and immersion time (p-r).

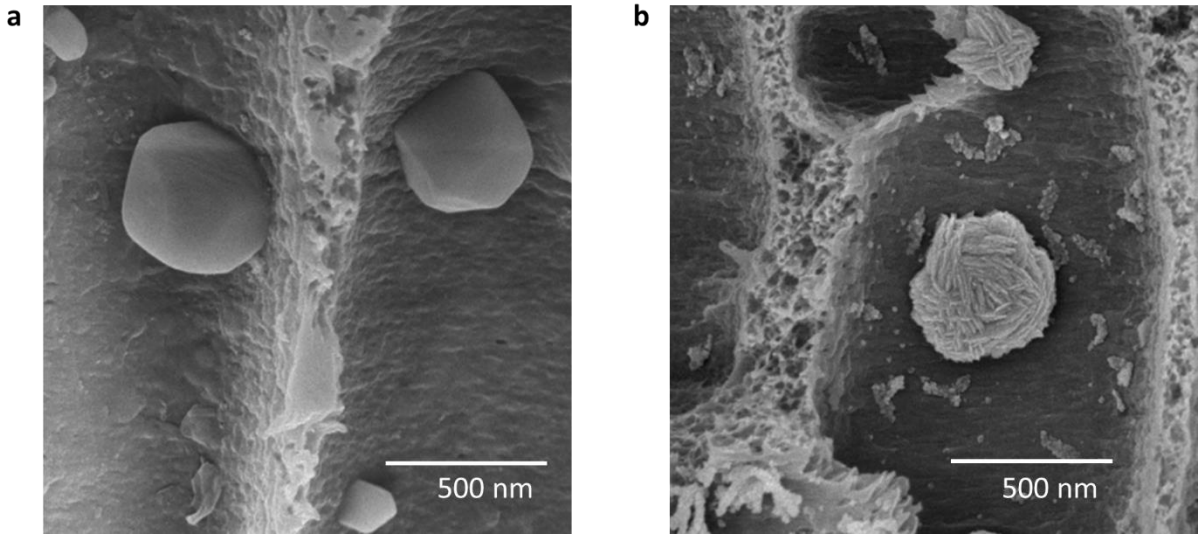

Fig. S14. SEM images of the agglomerate formed in the membrane after treatments for 1 week (a) and 1 month (b). The morphology of the agglomerate after the 1-month treatment is similar to the shape of desert rose selenite.

Fig. S15. The photos of "Selenite (desert) roses" by Orbital Joe were licensed under CC BY-NC-ND 2.0.

Table S1. Elemental analysis of the membranes.

Membranes	wt.%			
	C	N	Cu	I
M0	77.9	18.2	0	0
M1	77.7	17.1	0	0
M2	75.7	17.4	2.12	3.86
M3	64.2	14.0	7.56	14.21

Table S2. Membrane stability test conducted by soaking the membranes in different solvents for 24 h.

Membranes	Heptane	Toluene	DMSO	Ethanol	THF	DMF	DMAc	Acetone	Methanol	Acetonitrile
M0	✓	✓	✗	✓	✓	✗	✗	✓	✓	✓
M1	✓	✓	✗	✓	✓	✗	✗	✓	✓	✓
M2	✓	✓	✗	✓	✓	✗	☒	✓	✓	✓
M3	✓	✓	✓	✓	✓	✓	✓	✓	✓	✓

✓ Membrane resists, very opaque color, solution appears fairly clear.

☒ Membrane is partially dissolved, solvent color is slightly greenish.

✗ Membrane is totally dissolved, PP support floats, solvent color is yellowish.

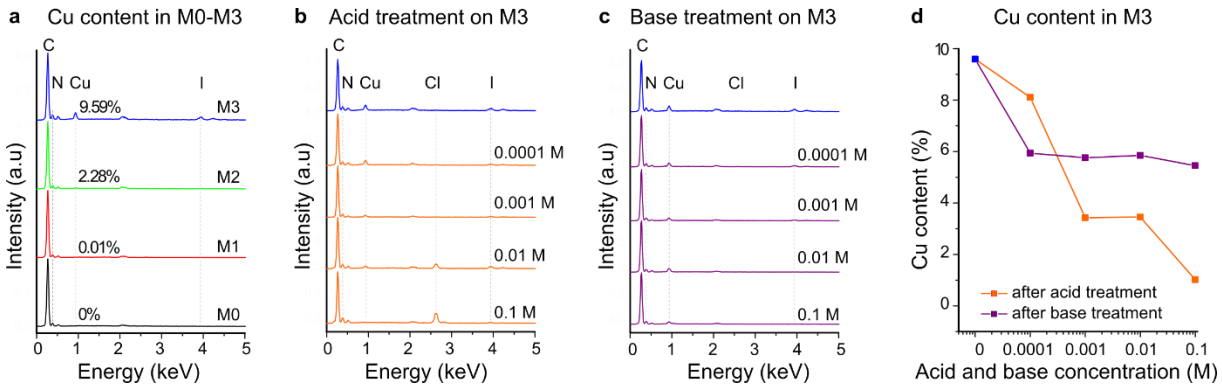

Fig. S16. EDX spectra of M0-M3 (**a**), M3 after immersion in acid at various concentrations (**b**), M3 after immersion in base at various concentration (**c**). Cu content in the M3 after immersion in acid and base at various concentration (**d**).

2. Pore size calculation

Table S3. Physical properties of acetone [1].

Solvent	M_w[a] (Da)	d_m[b] (nm)	H[c] (mPa s)	V_m[d] ($cm^3\ mol^{-1}$)	ρ[e] ($g\ ml^{-1}$)	δ_d[f] ($MPa^{0.5}$)	δ_P[g] ($MPa^{0.5}$)	δ_h[h] ($MPa^{0.5}$)	δ_t[i] ($MPa^{0.5}$)
Acetone	58.08	0.308	0.316	74.166	0.784	15.5	10.4	7.0	19.9

[a] Molar mass; [b] diameter; [c] dynamic viscosity; [d] molar volume; [e] density; [f,g,h,I] Hansen parameters (dispersion, polar, hydrogen bonding and total, respectively).

As suggested by Livingston et al. [2], the permeance of a solvent can be correlated using its physical properties. The acetone diameter was calculated as follows:

$$d_{\mathrm{m}} = 2 \cdot \left(\frac{3V_m}{4\pi N_A}\right)^{\frac{1}{3}}, \quad \text{S1}$$

where V_{m} is the molar volume obtained from the solvent density, and N_A is Avogadro's number. The Hagen–Poiseuille equation defines the volumetric flux (J_v) through a membrane comprising uniform capillaries:

$$J_{v,i} = \frac{r_i^2 \Delta P \varepsilon}{8\mu_0 l}, \quad \text{S2}$$

where ε is the porosity, ΔP is the transmembrane pressure, l is the capillary length, μ_0 is the solvent bulk viscosity, and r_i is the capillary radius. Next, using the pore flow rate ($Q_{p,i}$), the flow through a pore of radius r_i could be calculated as follows:

$$Q_{p,i} = \frac{\pi r_i^4 \Delta P}{8\mu_0 l}. \quad \text{S3}$$

The overall solute rejection could be calculated using the following equation:

$$R_{ij} = 1 - \frac{\Phi_{ij} K_{c,ij}}{1 - \left(1 - \Phi_{ij} K_{c,ij}\right)\left(\exp(-P_{e,ij})\right)}, \quad \text{S4}$$

where Φ_{ij} is the partition coefficient, and λ_{ij} is the ratio between the solute radius $r_{s,j}$ (the subindex for a solute is j) and pore radius r_i (the subindex for a pore-size-class in the discrete method is i):

$$\Phi_{ij} = \left(1 - \lambda_{ij}\right)^2, \quad \text{S5}$$

$$\lambda_{ij} = \frac{r_{s,j}}{r_i}. \quad \text{S6}$$

Assuming that a steric interaction occurred between the solute and pore walls, the solute convective $K_{c,ij}$ and diffusive $K_{d,ij}$ hindrance factors were expressed as follows:

$$K_{c,ij} = \left(2 - \Phi_{ij}\right)\left(1 + 0.054\lambda_{ij} - 0.988\lambda_{ij}^2 + 0.44\lambda_{ij}^3\right), \quad \text{S7}$$

$$K_{d,ij} = 1 - 2.3\lambda_{ij} + 1.154\lambda_{ij}^2 + 0.224\lambda_{ij}^3. \quad \text{S8}$$

The Peclet number ($P_{e,ij}$) characterizing the pore flow was defined as

$$P_{e,ij} = \frac{K_{c,ij}}{K_{d,ij} D_{s,j}} \left(\frac{r_i^2 \Delta P}{8\mu_{p,i}} \right). \quad \text{S9}$$

The diffusivity $D_{s,ij}$ of a solute of radius $r_{s,j}$ was calculated using the Stokes–Einstein equation:

$$D_{s,ij} = \frac{kT}{6\pi\mu_{p,i} r_{s,j}}, \quad \text{S10}$$

where k is the Boltzmann constant and T is the temperature. The Wilke–Chang formula could be used to solve the above equation and estimate the solute's diffusivity:

$$D_{s,ij} = 7.4 \times 10^{-8} \frac{T\sqrt{\phi M_{solv}}}{\mu_{p,i} V_{m,j}^{0.6}}, \quad \text{S11}$$

where M_{solv} is the molecular weight (M_w) of the solvent molecule, ϕ is a dimensionless solvent parameter, and $V_{m,j}$ is the solute molar volume (in cm^3 g mol^{-1}). If the rejection value $R(r)$ is a continuous function of the pore radius r, then PDF $f_R(r)$ is introduced to describe the pore size distribution:

$$f(r) = \frac{1}{r\sqrt{2\pi b}} \exp\left[-\frac{\left(\log(r/r^*) + b/2\right)^2}{2b} \right], \quad \text{S12}$$

where

$$b = \log\left[1 + \left(\frac{\sigma}{r^*} \right)^2 \right]. \quad \text{S13}$$

To calculate function $f(r)$, the mean pore radius (r^*) and its standard deviation (σ) had to be estimated. For simplification, the distribution function was truncated to r_{max}:

$$\frac{f'_R(r)}{f_R(r)} = \frac{1}{\int_0^{r_{max}} f_R(r) dr}. \quad \text{S14}$$

The overall rejection value over the pore radii of $0 < r < r_{max}$ could then be calculated as

$$R_j = \frac{\int_0^{r_{max}} f'_R(r) r^4 R(r)/\mu(r) dr}{\int_0^{r_{max}} f'_R(r) r^4/\mu(r) dr}. \quad \text{S15}$$

By implementing the above models, the mean pore size and its standard deviation could be fitted by minimizing the error.

Table S4. Physical properties of the solvents and their solvent solubility parameters.

Solvents	Abbreviation	M_w[a] (g mol^{-1})	d_m[b] (nm)	η[c] (mPa s)	V_m[d] (cm^3 mol^{-1})	ρ[e] (g ml^{-1})	δ_d[f] (MPa$^{0.5}$)	δ_P[g] (MPa$^{0.5}$)	δ_h[h] (MPa$^{0.5}$)	δ_t[i] (MPa$^{0.5}$)	δ_p (η d_m^2)
Heptane	Hep	100.2	0.776	0.41	147.5	0.664	15.3	0	0	15.3	0
Toluene	PhMe	92.1	0.697	0.59	106.26	0.867	18	1.4	2	18.16	4.89
Ethanol	EtOH	46.1	0.52	1.07	44.13	1.044	18.4	6.3	13.7	23.79	21.71
ethyl acetate	EtOAc	88.1	0.677	0.46	97.68	0.902	15.8	5.3	7.2	18.15	25.1
Tetrahydrofuran	THF	72.1	0.637	0.48	81.11	0.889	16.8	5.7	8	19.46	29.29
dimethyl carbonate	DMC	90.1	0.645	0.59	84.7	1.073	15.5	8.6	9.7	20.21	35.07
dimethylformamide	DMF	73.1	0.626	0.8	77.1	0.948	17.4	13.7	11.3	24.86	43.58
Dichloromethane	DCM	84.9	0.588	0.41	64	1.327	18.2	6.3	6.1	20.2	44.06
Methylethylketone	MEK	75.1	0.667	0.43	93.3	0.805	16	9	5.1	19.05	47.02
Methanol	MeOH	32	0.505	0.55	40.45	0.792	15.1	12.3	22.3	29.61	88.5
Acetone	AcMe	58.1	0.618	0.3	74.08	0.784	15.5	10.4	7	19.94	92.36

3. Membrane performance

Table S5. Rejection of the dyes and APIs for M3 in acetone at 30 bar.

API and dyes	Abbreviation	Molecular weight (g mol^{-1})	Rejection (%)	Std. Dev.
Estradiol	ED	272.38	91.10	1.25
methyl orange	MO	327.33	91.30	0.80
Losartan	LS	422.92	94.23	1.22
Valsartan	VS	435.52	94.13	1.53
Oleuropein	OR	540.51	97.07	0.65
Acid fuchsin	AF	585.54	99.27	0.21
Roxithromycin	RT	837.05	100.00	0.00
Rose bengal	RB	1017.65	100.00	0.00

Table S6. Flux of acetone through M0-M3 at 30 bar.

Pressure (bar)	Flux (L m^{-2} h^{-1})				Std. Dev.			
	M0	M1	M2	M3	M0	M1	M2	M3
0	0.00	0.00	0.00	0.00	0.00	0.00	0.00	0.00
10	69.67	50.33	39.33	19.67	8.08	4.04	3.51	6.51
20	179.67	141.33	103.00	47.67	9.07	10.26	11.14	6.43
30	250.33	211.67	158.00	72.67	8.62	8.74	8.54	8.02
40	294.00	254.00	203.00	92.00	9.17	10.82	12.53	11.53

Table S7. Comparison of the filtration performance of metal-polymer coordination membranes. NA = Information Not Available.

Literature	Year	Polymer matrix	Metal used	Metal concentration	Complexation solvent	Permeance (L m^{-2} h^{-1} bar^{-1})	Tested pressure (bar)	Tested solvents	Duration of the longest filtration	Acid/base stability	MWCO (g mol^{-1})	Solute rejection (%)	Solutes	Molecular weight of the solute (g mol^{-1})
Peinemann et al, Nano Lett. 15, 3166-3171	2015	Polythiourea (PTU)	Ni	2.5–10 mM	DMSO	0.005	NA	water	NA	NA	NA	99	safranin	351
												99	brilliant blue	826
			Cu	2.5–10 mM	DMSO	0.033	NA	toluene	NA	NA	NA	88	protoporhyrin IX dimethyl ester	590
			Pd	2.5–10 mM	DMSO	0.09	NA	water	NA	NA	NA	87	safranin	351
												98	brilliant blue	826
Nunes et al, Chem. Commun. 53, 6609	2017	Poly(acrylic acid)-b-Polusulfone-b-Poly(acrylic acid)	Cu	100 mM	water	0.15	8	water	12 h	yes	7000	21	NaCl	58
												83	$MgCl_2$	95
			Ag	100 mM	water	NA	8	water	12 h	NA	NA	NA	NA	-
Our work	2021	Polybenzimidazole (PBI)	Cu	1000 ppm (5 mM)	MeCN	1.97	10	acetone	13 days	yes	357	91	Estradiol	272
												91	methyl orange	327
												94	Losartan	423
												94	Valsartan	435
												97	Oleuropein	540
												99	Acid fuchsin	585
												100	Roxithromycin	837
												100	Rose bengal	1017

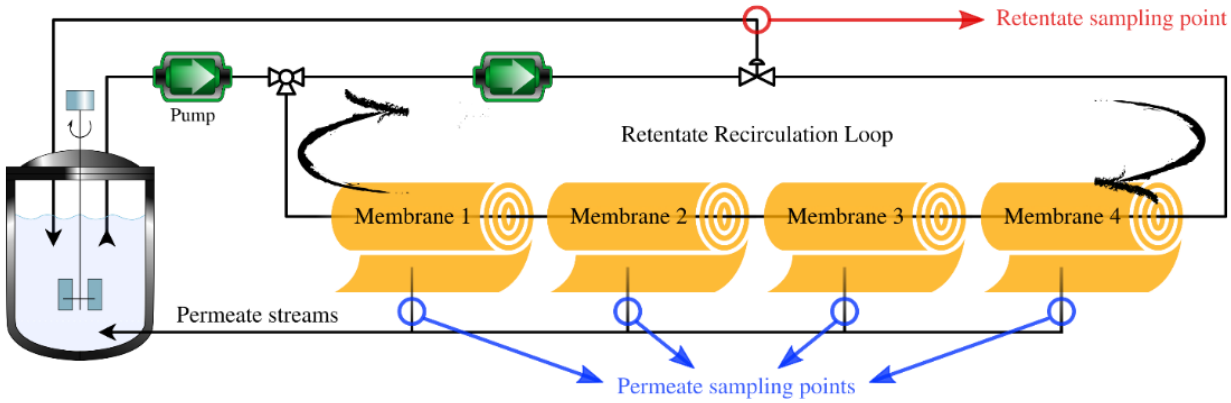

Fig. S17. Schematic of the multistage crossflow nanofiltration apparatus used for membrane testing.

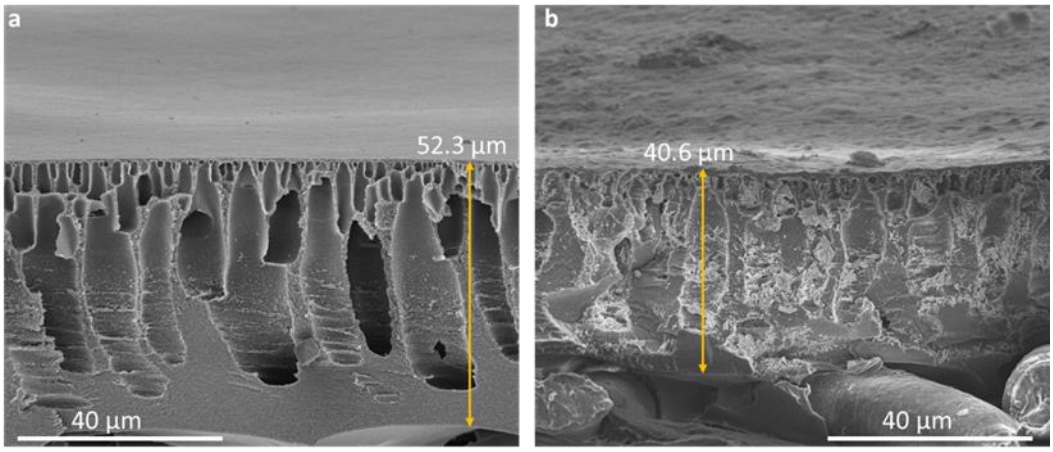

Fig. S18. SEM cross-section of M3 before (a) and after (b) continuous filtration test.

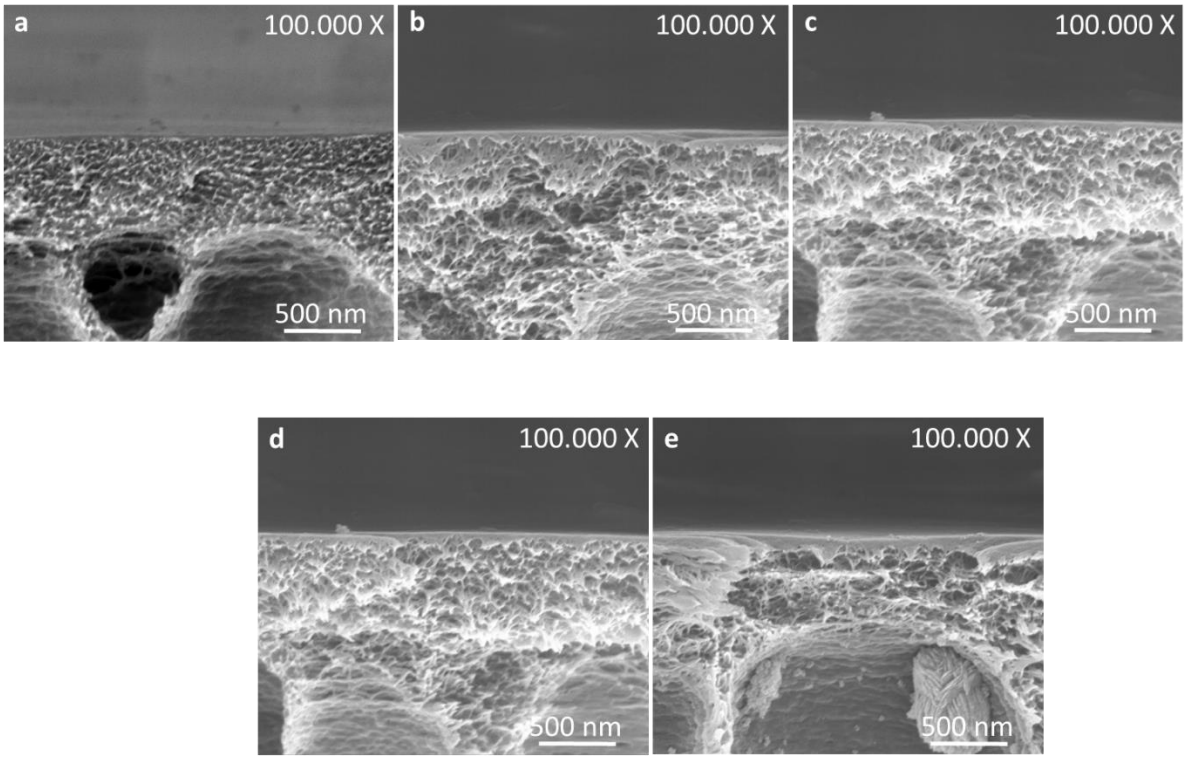

Fig. S19. High magnification of SEM cross-section of M1 (a), M2 (b) and M3 (c) to observe there is no difference on the top layer thickness as a function of CuI concentration. The cross-section of M3 (d) and M3 after immersion time of 1 month (e) is compared to show there is no significant difference on the top layer thickness caused by various immersion time.

4. Reference

[1] S.-H. Park, A. Alammar, Z. Fulop, B. Pulido, S. Nunes, G. Szekely, Green Chem. (2020).
[2] S. Karan, Z. Jiang, A.G. Livingston, Science 348 (2015) 1347–1351.